# Balancing Performance and Efficiency in a Robotic Fish with Evolutionary Multiobjective Optimization

Anthony J. Clark*, Jianxun Wang†, Xiaobo Tan†, and Philip K. McKinley*
*Department of Computer Science and Engineering
†Department of Electrical and Computer Engineering
Michigan State University, East Lansing, MI, USA
ajc@msu.edu

***Abstract*—In this paper, we apply evolutionary multiobjective optimization to the design of a robotic fish with a flexible caudal fin. Specifically, we use the NSGA-II algorithm to discover solutions (physical dimensions, flexibility, and control parameters) that optimize both swimming performance and power efficiency. The optimization is conducted in a custom simulation environment based on an accurate yet computationally-efficient model of hydrodynamics. The results of these simulations reveal general principles that can be applied in the design of robotic fish morphology and control. To verify that the simulation results are physically relevant, we selected several of the evolved solutions, fabricated flexible caudal fins using a multi-material 3D printer, and attached them to a robotic fish prototype. Experimental results, conducted in a large water tank, correspond reasonably well to simulation results in both swimming performance and power efficiency, demonstrating the usefulness of evolutionary computation methods to this application domain.**

## I. Introduction

Similar to live fish, robotic fish accomplish swimming by deforming their bodies or fin-like appendages. This form of locomotion offers certain key advantages relative to traditional propeller-driven underwater vehicles. First, robotic fish are potentially more maneuverable, which is critical when operating in cluttered underwater environments [1], [2]. Second, since robotic fish produce very low acoustic noises and exhibit wake signatures similar to live fish, they are less intrusive to aquatic ecosystems and offer stealth in security-related applications. Third, robotic fish require fewer active mechanical components, such as servomotors, which leads to designs with fewer sources of failure. Finally, with fin/body movements at relatively low frequencies (typically a few Hz), these systems are less likely to harm aquatic animals or become jammed with foreign objects.

Yet, the characteristics of current materials and electromechanical components mean that even robots precisely modeled after their natural counterparts will not be nearly as capable. One approach to improving performance is integrating flexible materials into the morphology (body) of a robot. Passive, flexible components are intended to partially compensate for actuation capabilities that are primitive relative to those of biological organisms. However, integrating such materials into a robot poses numerous challenges in controlling the system, since the flexibility of a structure affects the resulting forces and moments experienced during interactions with the environment [3]–[5]. The increased design complexity can be addressed in part with the help of rapid prototyping equipment, such as 3D printers, which can decrease the time between design and physical testing [6]. Further, recent advances in 3D printing technology allow for multiple materials to be jetted simultaneously, which has enabled the printing of composite materials as done in this study.

When optimizing a robotic fish, the primary objective is typically to improve swimming performance in terms of both speed and maneuverability. However, energy efficiency is also of concern in many applications. For example, robotic fish used in mobile sensor networks may need to be small or compact and thus operate with limited power resources (i.e., a small battery pack). In this study, we consider efficiency as the ratio between useful power and total mechanical power exerted by the caudal fin (these terms are defined in Section III). To improve both swimming performance and efficiency is challenging due to the competitive nature of these two objectives.

Finding solutions that effectively balance these concerns is the focus of this paper. Evolutionary multiobjective optimization (EMO) algorithms [7], [8] are well suited to such problems because they converge to a *set* of Pareto-optimal solutions, as opposed to only a single optimum. The set of optimal solutions belonging to a Pareto front are said to be *nondominated*; that is, each of the solutions is optimal in some respect. For this study, we instantiate the NSGA-II algorithm [7], which is widely used in both research and real-world applications.

In this study, we optimize both control and morphology of a robotic fish with a flexible caudal fin, shown in Figure 1, against two objectives: maximal average speed and power efficiency. Evolved results are then fabricated with the aid of a multi-material 3D printer, and physically validated. The methods developed in this study are intended to support the design of robotic fish for practical applications such as remote sensor networks. More broadly, the techniques presented in this study are expected to be applicable to the design of other robots containing flexible components.

## II. Background and Related Work

As an emerging class of embedded computing system, robotic fish are anticipated to play an important role in environmental monitoring [1], inspection of underwater structures [9], tracking of hazardous wastes and oil spills [10],

978-1-4799-4479-8/14/$31.00 ©2014 IEEE

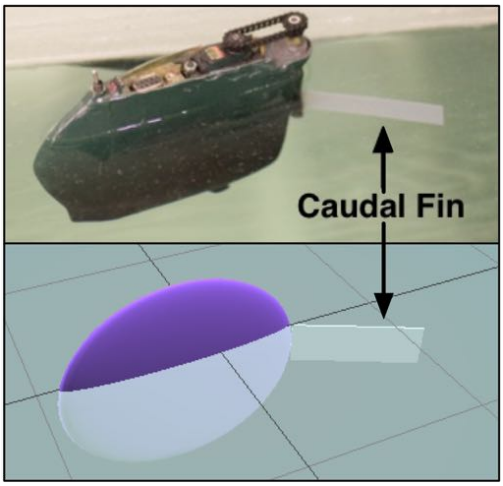


Fig. 1. (top) The robotic fish prototype used in this study, and (bottom) the virtual representation evolved during simulation.

and the study of natural systems [11], [12]. However, while studies of robotic fish have produced many advances over the past two decades [13]–[15], robotic fish still do not approach their biological counterparts in terms of swimming abilities.

Integrating flexible materials as fins, or as entire bodies, is one approach to improving performance [16], [17], but also increases design complexity. Clark et al. [4] have demonstrated how evolutionary computation (specifically, a genetic algorithm) can be applied to optimize both morphological characteristics and control patterns in robotic fish. However, the above studies are concerned only with increasing swimming performance, such as thrust, speed, or maneuverability. Most practical applications also require a robotic fish to perform such behaviors *efficiently*.

Several studies have addressed the design of aquatic robots with flexible components [3], [18], [19]. However, unlike the work presented here, most use either a simulation-only or parametric design approach. For example, Low et al. [20] used statistical methods to investigate the effect of control and morphological design parameters on the resulting thrust of a robotic fish with a flexible caudal fin. In [21], Esposito et al. performed a similar analysis of a caudal fin with six independently actuated fin rays. While studying a single kinematic parameter, the phase difference between the driving angle at the base of a flexible caudal fin and the fin-bending angle, Park et al. [18] discovered that maximal thrust occurs at the same phase difference, even when the morphology of the caudal fin is changed. Different from these studies, our work is concerned with maximizing *both* thrust, which is necessary for maximizing average speed, and efficiency with an evolutionary algorithm.

As noted above, EMO algorithms are applicable when the tradeoffs among competing/conflicting objectives need to be balanced during optimization. EMO algorithms typically use an elitism approach for driving solutions toward the optimal Pareto front, and a niching or crowding mechanism to ensure that the entire set of Pareto-optimal solutions can be found [7], [8]. The advantages of EMO algorithms, when compared to single objective evolutionary algorithms and typical parameter sweeps, include: (1) locating a Pareto front with fewer evaluations, (2) automatically handling constraints, (3) not having to specify the relative importance among multiple objectives, and (4) automatically sorting solutions according to feasibility and domination.

The remainder of the paper is organized as follows. In Section III we describe the modeling and simulation of robotic fish, followed in Section IV by the details of fabricating and testing flexible caudal fins. In Section V, we present the results of evolutionary optimization runs, and in Section VI the results of physical validation experiments. Finally, we present our conclusions in Section VII.

## III. Modeling and Simulation

Evolutionary optimization is often conducted with the aid of a simulation environment, which provides a means to conduct a large number of evaluations in a short amount of time. The main drawback of simulation lies with the so-called *reality gap* [22], which arises when solutions that appear to work well in a simulated environment perform differently in a physical environment. In this study, we use a dynamics model developed by Wang et al. [23] based on Lighthill's Large-Amplitude Elongated Body Theory of Locomotion [24]. This model has proven to be both accurate and computationally efficient [4], [23]. In general, higher accuracy simulations tend to have a better chance of *crossing* the reality gap [25].

### A. Dynamics

Simulation of the robotic fish is conducted in Simulink [26], which allows for a straightforward translation of dynamic equations (described below) into simulation. Wang's model assumes that all motion is constrained to a two-dimensional plane, and is based on the *added mass effect*, for which rigid bodies appear more massive due to surrounding water. Specifically, the dynamic model calculates thrust forces as if a volume of water were pushing on the fin in direct opposition to its motion.

A critical aspect of simulation is the modeling of the flexible caudal fin dynamics, as illustrated in Figure 2. Flexibility is modeled as multiple rigid segments connected by springs and dampers. The spring coefficient between two consecutive segments depends on how stiff or flexible the caudal fin should behave.

The force acting on each fin segment $f_i$ can be calculated independently with:

$$\vec{f}_i(\tau) = \begin{pmatrix} f_{i,x}(\tau), \\ f_{i,y}(\tau) \end{pmatrix} = -m\frac{d}{dt}(v_\perp \hat{n}), \qquad (1)$$

where $m$ denotes mass per unit length, $\tau$ is the location on the fin where the force acts, and $\hat{n}$ and $v_\perp$, respectively, are the unit direction and velocity perpendicular to the fin. The tip of the final segment experiences an additional force described by:

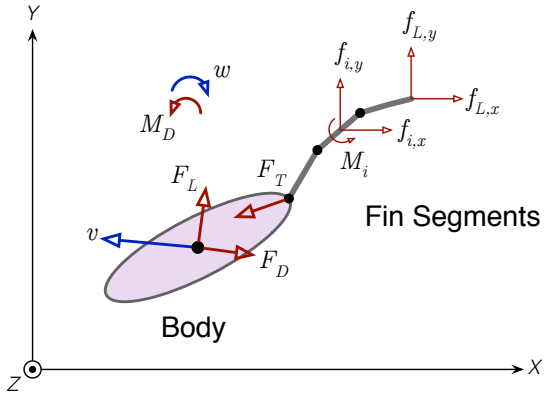


Fig. 2. Graphical representation of the simulated hydrodynamics for a robotic fish with a rigid body and flexible caudal fin. Linear velocity $v$ and angular velocity $w$ are the result of thrust force $F_T$, drag force $F_D$, lift force $F_L$, and drag moment $M_D$. $F_T$ is calculated as the sum of all forces acting on the fin segments.

$$\vec{f_L} = \begin{pmatrix} f_{L,x} \\ f_{L,y} \end{pmatrix} = \left[ -\frac{1}{2} m v_\perp^2 \hat{m} + m v_\perp v_\parallel \hat{n} \right]_{\tau=L}, \quad (2)$$

where $\tau$=L represents the posterior end of the fin, and $\hat{m}$ and $v_\parallel$, respectively, are the unit direction and velocity parallel to the fin. The resulting thrust force $F_T$ is simply a summation of all segment forces $f_i$ and the tip force $f_L$. In our simulations, the caudal fin is modeled with 5 segments.

### B. Evolutionary Optimization

The dynamic simulation described above is parameterized by several terms, including the amplitude and frequency of a sinusoidal control signal and the length, height, and flexibility (spring and damping coefficients) of the caudal fin. The range for each of these values, aside from the spring coefficient, is listed in Table I.

TABLE I
RANGE OF EVOLVED PARAMETERS

| | Min | Max |
|---|---|---|
| Amplitude ($rad$) | 0.08 | 0.5 |
| Frequency ($Hz$) | 0.5 | 3.0 |
| Fin Length ($cm$) | 3 | 15 |
| Fin Height ($cm$) | 1 | 5 |
| Young's Modulus ($GPa$) | 0.1 | 3 |

Unlike the other parameters, the range of spring coefficient values is not chosen by a designer. Instead, it is limited by the properties of available materials. For this study, the spring coefficient is restricted to what our 3D printer, an Objet Connex350, is capable of fabricating. Moreover, for physical materials it is more common to consider their Young's modulus, an inherent material property relating to elasticity and flexibility measured in Pascals (Pa). Consequently, this quantity is displayed in the table in place of a range for spring coefficients. The printed materials, and resulting Young's modulus range, are discussed in Section IV.

For evolving genomes comprised of real values, NSGA-II requires a user to set the four following parameters (values are in parenthesis): the probabilities of crossover (90%) and mutation (33%), and the distribution index for both simulated binary crossover (10) and polynomial mutation (10).

### C. Constraints

Along with evolving the parameters as real-valued numbers, NSGA-II also accommodates the following two limitations. First, the dynamic model described above is only valid for an elongated fin in which fin length is at least roughly three times the fin height (Eq. (3)). Second, the dynamic model itself does not place any limitation on power supplied at the base of the caudal fin, presumably by a servomotor, so we include a maximum power constraint (Eq. (4)). Practically, the maximum power constraint limits the top speed of the robotic fish. So, we have:

$$length - 3height \geq 0 \quad (3)$$

$$MAX\_POWER - power \geq 0 \quad (4)$$

where $length$, $height$, and $power$ refer to the robotic fish caudal fin, and the maximum power constant $MAX\_POWER$ was determined experimentally. In NSGA-II these limitations are treated as constraints, which enables the algorithm to smoothly follow a gradient from *infeasible* (i.e., a solution that violates a constraint) to *feasible* solutions.

### D. Fitness Evaluation

Each evolved individual is evaluated for 10 seconds of simulation time, however, only the second half of this period determines fitness. This allows the robotic fish to reach a cruising speed and final heading, with average speed and power efficiency calculated over the final 5 seconds. Power efficiency is the ratio of two terms: *effective power* as the numerator, and *total power* as the denominator. Both of these terms are mechanically based (as opposed to the electrical power of the motor) and are calculated using Equations (1), (2), and the following definition of mechanical power:

$$\vec{P}(t) = \vec{F}\vec{v}, \quad (5)$$

where $\vec{P}$ is mechanical power, and $\vec{F}$ and $\vec{v}$ can be taken as the instantaneous force and velocity, respectively, of a point on the caudal fin.

Effective power, sometimes called *useful power*, is illustrated in Figure 3. Effective power takes the robotic fish's velocity and total force and projects it along the average direction of motion (labeled $d_{5to10s}$) before using (5) to calculate an average power. Practically, effective power includes only the surge (forward-to-back) force produced by the caudal fin. Total power, on the other hand, includes the force exerted to create *both* sway (side-to-side) and surge motions. The resulting power efficiency ratio has a range from 0 to 100%.

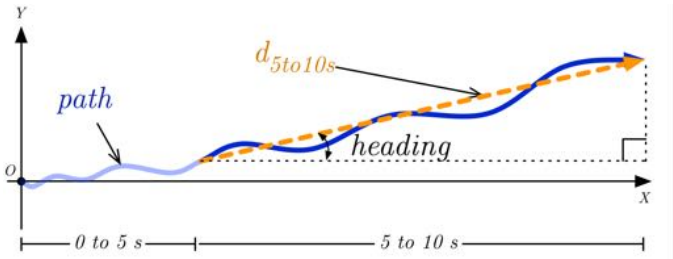


Fig. 3. An illustration of the dynamics involved in calculating fitness. The $path$ of the robotic fish includes two parts: a light-blue segment from 0 $to$ 5 seconds, which does not directly affect fitness, and a dark-blue segment from 5 $to$ 10 seconds used to evaluate fitness. The path settles to an average $heading$, which is not in line with the X-axis, due to a bias caused by the initial rotation of the caudal fin. The dashed, orange line ($d_{5to10s}$) represents displacement over the final 5 seconds of simulation.

## IV. Fin Fabrication and Testing

In simulation, flexibility of the caudal fin is determined by spring coefficients. As discussed above, however, the flexibility of real materials is expressed as a physical property such as the Young's modulus. As a result, we require the following equation, which relates a spring coefficient to the Young's modulus of a 3D-printed material:

$$K_s = \frac{Edh^3}{12l}, \tag{6}$$

where $K_s$ and $E$ refer to spring coefficient and Young's modulus values, respectively, and $d$, $h$, and $l$ represent the height, thickness, and length of a material, respectively. Equation (6) allows us to fabricate a simulated caudal fin.

To match the Young's modulus of printed materials with evolved spring coefficients, we designed composite fins in which flexibility is adjusted by varying the relative thickness of two different materials, as shown in Figure 4. The fin comprises two outer layers of a rubber-like TangoBlackPlus polymer, and an inner layer of a more rigid VeroWhitePlus material. When discussing composite materials, flexibility is often referred to as an *effective* Young's modulus to distinguish from uniformly fabricated materials. Specifying the thickness of the inner layer, $t_{inner}$, and fixing the overall thickness to 1.2 mm provides a set range of possible effective Young's modulus values.

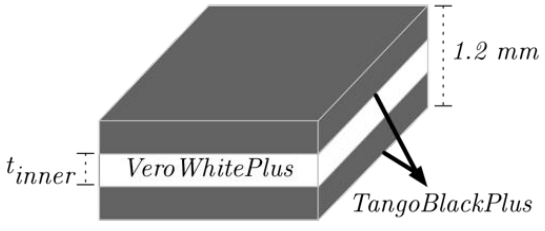


Fig. 4. Diagram of a composite material for a 3D-printed flexible caudal fin. The overall thickness is a constant 1.2 mm. The effective Young's modulus value for the composite material depends on the relative thickness ($t_{inner}$) of the inner VeroWhitePlus layer with respect to the two flexible TangoBlackPlus outer layers. In this diagram, a fin would be lying on its side.

To determine the 3D-printable range of effective Young's modulus values, we set up the experiment shown in Figure 5(a), and evaluated values of the Young's modulus for a series of composite materials with different values of $t_{inner}$. For this experimental setup, $E$ is evaluated with:

$$E = \frac{L_b^3 P_L}{3 I_b w_L} \tag{7}$$

where $L_b$ and $I_b$ are the length and area of moment inertia of the test composite, respectively, and $P_L$ and $w_L$ are the load and displacement at the tip of the composite, respectively.

As shown in Figure 5(b), a sample-size composite material is fixed to a harness while its tip rests against a load cell. Displacement at the tip is adjusted using a sliding rail and measured with a laser sensor. Three replicate sets of load and displacement data are gathered for each composite material, in which each set comprises five data points at different displacements. A least square error method is adopted to find the slope between force and displacement for each of the three sets, and the effective Young's modulus for each composite is evaluated as the average of the three replicate experiments.

Figure 6 shows the results of these experiments for different values of $t_{inner}$. As shown, the evolvable range of spring coefficients corresponds to an effective Young's modulus of approximately 100 MPa to 3 GPa. This roughly gives a range of materials from rubber, which typically has a Young's modulus of 10 to 100 MPa, to hard plastics, which have a Young's modulus of 1 to 5 GPa. The *best fit* line in Figure 6 can be utilized to find the required $t_{inner}$ value for a given Young's modulus.

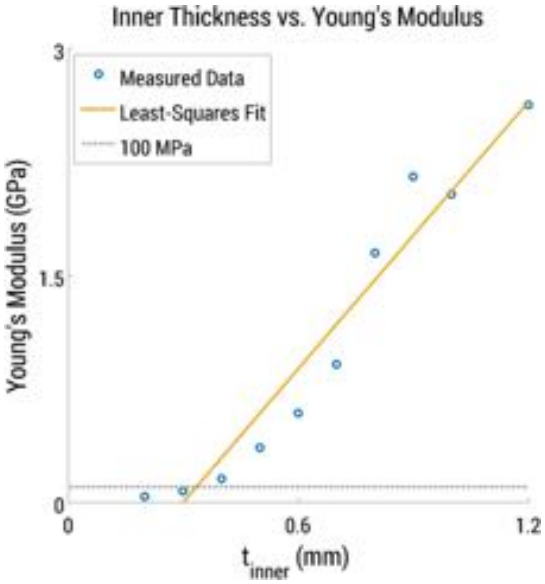


Fig. 6. Effective Young's modulus of composite materials for different values of $t_{inner}$.

## V. Results and Discussion

We conducted 20 replicate evolutionary runs, each containing 200 individuals evolving for 500 generations. All of the 20 replicates converged to a similar Pareto front. In total, each

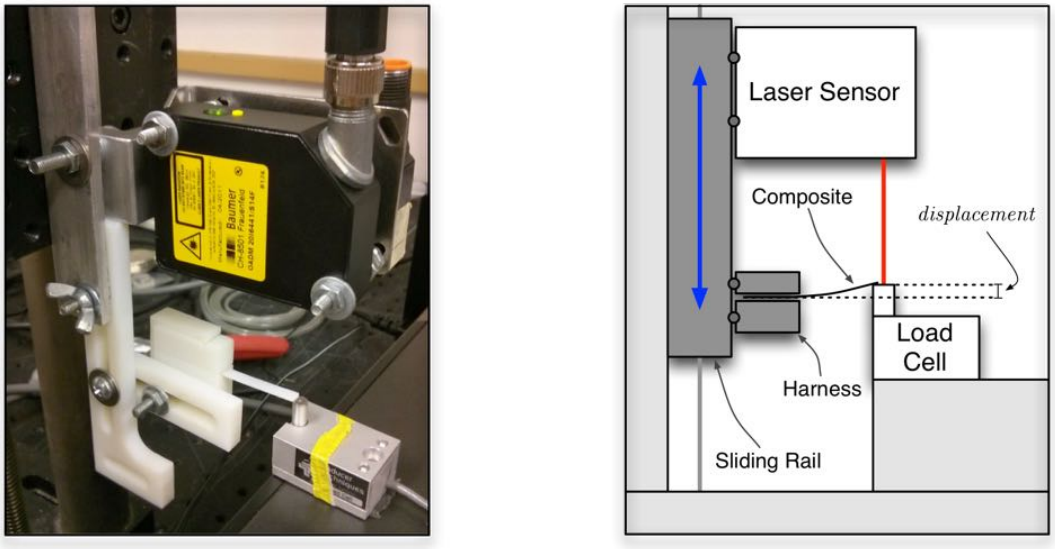


(a) (b)

Fig. 5. Testing of physical fins. (a) Photograph of the experimental setup for measuring the effective Young's modulus of 3D-printed composite materials. (b) Diagram of the same experiment showing the testing process.

replicate simulation requires roughly $5 \times 10^4$ evaluations to converge to a final Pareto front, which is significantly less than what could be required for a parameter sweep over the same parameter ranges. For example, testing each of the 6 parameters (i.e., the 5 parameters shown in Table I and an additional spring damping coefficient) at 10 evenly distributed points would require exactly $10^6$ evaluations. Furthermore, unlike an EMO algorithm, such a parameter sweep would not evaluate values in between the 10 fixed points, resulting in a more coarse optimization.

Figure 7 shows the combined Pareto front for the 20 replicate runs. The combined Pareto front reveals that for our robotic fish prototype an optimal caudal fin and control signal can produce a maximum average speed (given the maximum power constraint) in the range of approximately 4.8 to 5.8 cm/s and an efficiency in the range of 35 to 42%. As expected, we see that an increase in speed is accompanied by a decrease in efficiency. Although the Pareto front is clearly formed, it only covers a small range of values; particularly speed, which only varies by 1 cm/s. This effect can be seen in Figure 8, which shows every feasible solution evolved in each of the 20 replicate experiments. Each of the subsequent figures in this section will correspond to the data plotted in Figure 7.

Inspecting how each parameter affects each objective can give insight into how parameter values should be selected. For example, the two plots in Figure 9 show how the length of a caudal fin affects each of the two objectives. For length, it appears that values between 6 and 12 cm are effective; furthermore, higher values for length within this range produce higher speed, but decreased efficiency. A length in this range corresponds to roughly half the length of the body (14 cm), which is a common ratio for biological fish. These values for length depend on the additional parameters, but intuitively,

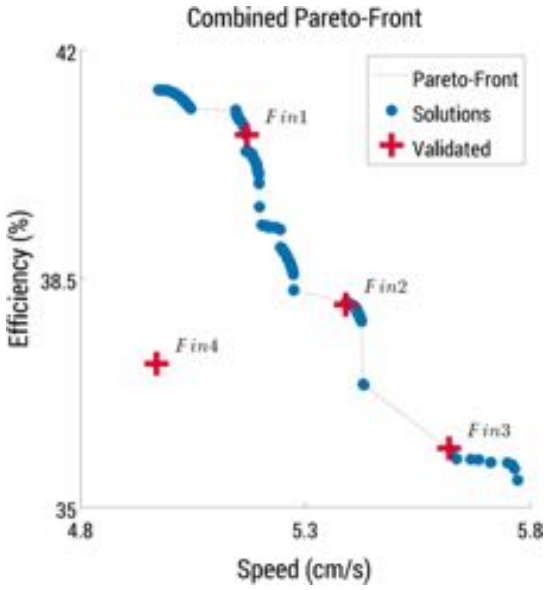


Fig. 7. A combined Pareto front including the best solutions from each of the 20 replicate evolutionary simulations. The labeled, red "+" symbols denote solutions that were physically fabricated and validated.

increasing the length of the fin should increase thrust, and therefore speed, at the cost of increased power usage.

Figure 10 demonstrates how each of the parameters converges in the combined Pareto front solutions (see Table I for the range of each parameter). In the figure, each parameter is scaled between 0 and 1 for an easier comparison. The lines between parameters connect values that belong to the same genome (evolved solution). The figure illustrates two important points. First, each parameter converges to a relatively small range of values, particularly fin flexibility (fins with a scaled value near 0 are very flexible). The evolution of flexible fins

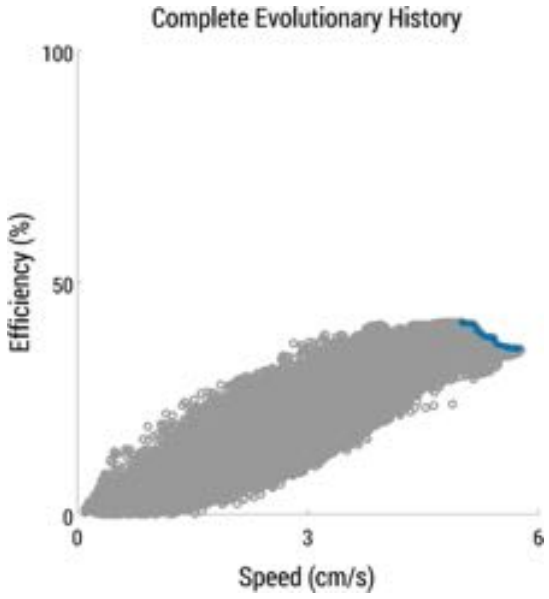


Fig. 8. The complete evolutionary history for each of the 20 replicate experiments. Every feasible, evolved solution is plotted, and the Pareto-front is highlighted in blue.

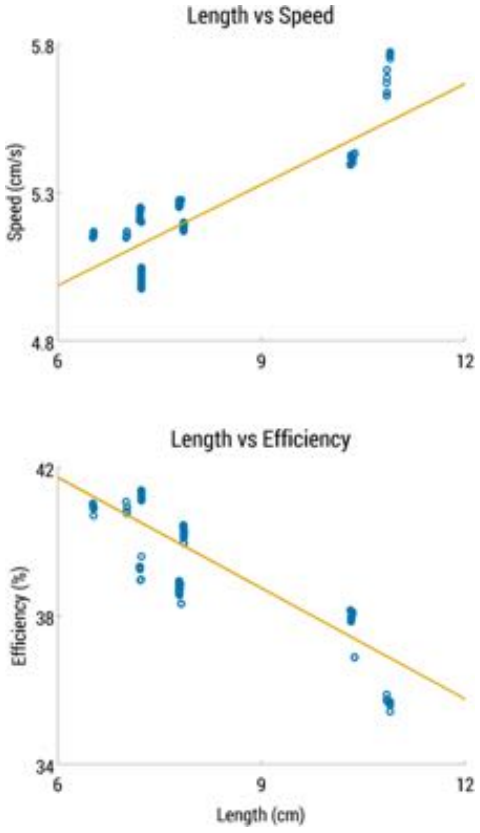


Fig. 9. Plots of evolved solutions showing relationships between fin length (x-axis) and the two objectives, speed (top) and efficiency (bottom). All Pareto-optimal solutions have a fin length between 6 to 12 cm, thus the x-axis does not include the entire evolvable range (3 to 15 cm).

is not unexpected, as a they produce higher thrust for lower values of control frequency and amplitude [4]. Second, most of the variation in the final population is in the length and height of the caudal fin.

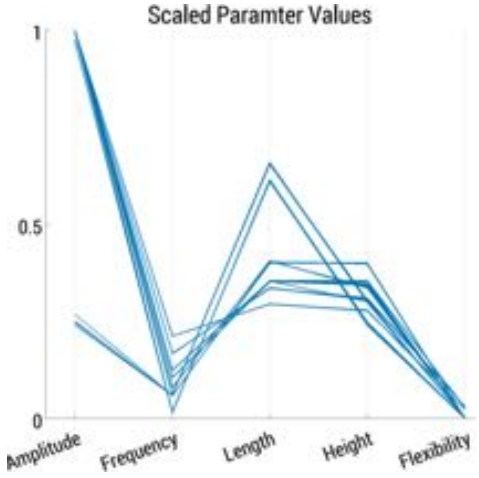


Fig. 10. The evolved parameters scaled between 0 and 1 for the combined Pareto front solutions.

Inspecting how close the evolved solutions come to violating the constraints (Equations (3) and (4)) can provide further insight into what constitutes a *good* design. For example, the constraint on fin dimensions sets a minimum length-height ratio of 3:1, and although the height and length parameters have a relatively high variation in the Pareto-optimal set, most converge to a similar ratio. More specifically, the best performing fins have a ratio less than roughly 3.5:1 (mean of 4.1 and median of 3.2), which signifies that while changes to the height and length can alter speed and efficiency, it is best to keep the ratio near 3:1 for better performance. Since our simulation environment does not allow for fins with a ratio of less than 3:1, physical testing will have to be conducted to determine whether lower values are more or less beneficial. Likewise, inspecting the constraint on maximum power shows that the best solutions utilize as much power as is allowed, which is important for generating the most thrust.

As for control of the caudal fin, Figure 10 indicates that it is better to increase the amplitude and decrease frequency of the sinusoidal motion. This can best be explained by examining the equations of motion for the caudal fin:

$$\theta(t) = Asin(2\pi Ft), \tag{8}$$

$$\dot{\theta}(t) = 2\pi AFcos(2\pi Ft), \tag{9}$$

$$\ddot{\theta}(t) = -4\pi^2 AF^2 sin(2\pi Ft), \tag{10}$$

where $A$ and $F$ are the amplitude and frequency of the sinusoidal motion, and $\theta$ is the angle of the caudal fin with respect to the body. Equation (10) demonstrates that caudal fin acceleration is proportional to the square of frequency, but only linearly proportional to amplitude. As shown by Equations (1) and (2), the resulting thrust, and thus the total power, is proportional to this same acceleration. Thus, the evolutionary convergence on high amplitudes and low frequencies suggests that higher frequencies require too much power, and that it is more effective to increase speed by increasing amplitude.

Our interpretation of Figure 10, along with the calculated caudal fin aspect ratio, provides the following general guidelines on how to produce an effective, efficient robotic fish. Specifically, the caudal fin should: (1) be relatively flexible (have a low Young's modulus), (2) have a fin length-height ratio close to 3:1, (3) have a fin length of roughly one-half the length of the body, and (4) increase thrust and speed by increasing the amplitude of motion rather than frequency.

## VI. Physical Validation

To verify that solutions evolved in simulation are physically meaningful, we selected four solutions from the combined Pareto front to fabricate and test (indicated by the labeled "+" symbols in Figure 7). Physical experiments use the same control and morphological parameter as their simulated counterparts. Making use of the best fit line from Figure 6 enables the 3D-printing of composite caudal fins with a specific evolved flexibility. For each chosen solution, a $t_{inner}$ value is calculated and a fin of the correct flexibility, length and height is printed. To compare the speed of virtual and physical fins, we attached the printed composite fin to the robotic fish prototype shown in Figure 1. This robotic fish was placed in a water tank and speed was measured and averaged over 5 trials, where each trial was conducted in the same manner as fitness is calculated for the virtual robot (described in Section III). Results of these physical experiments are summarized in Table II, where labels match those found in Figure 7. For three of the tested fins, these results show a reasonable correspondence between simulation and reality. $Fin1$, however, is notably faster in reality given the same parameters as simulation. We note that, the solutions on the Pareto front are clustered within a relatively small range of values for speed (as demonstrated in Figure 8). Effectively, all the fabricated fins produce good performance. As a consequence of this tight clustering, however, the trends among results for the physical experiments differ from those of the simulations. Additionally, imperfections introduced by the 3D printing process will amplify any disparity between simulation and reality (i.e., the reality gap).

TABLE II
Simulation-Reality Speed Comparison

| Label | Simulation (cm/s) | Reality (cm/s) |
|---|---|---|
| $Fin1$ | 5.17 | 7.43 |
| $Fin2$ | 5.39 | 4.00 |
| $Fin3$ | 5.62 | 5.00 |
| $Fin4$ | 4.97 | 4.90 |

When comparing virtual and physical results it is simple to compare their speeds, yet it is not as straightforward to validate power efficiency. However, since we are using mechanical power efficiency, the total power (denominator of power efficiency) of virtual and physical results will be approximately equal when both are controlled with the same frequency and amplitude and the caudal fin motions match.

As supported by Figure 11, the dynamic model utilized in this study is accurate with respect to the motion of the caudal fin. The figure demonstrates that for similar conditions (i.e., the same time point, control pattern, and fin morphology) the virtual and physical robotic caudal fins have the same behavior. Thus, it can be expected that total power between virtual and physical will be consistent with one another. To compare on the basis of power efficiency, we also require effective power (numerator of power efficiency). Since effective power is proportional to speed, the efficiency of virtual and physical trials can be compared by inspecting their average speeds. Accordingly, in Table II an increase in speed (from simulation to reality or vice versa) corresponds to an increase in efficiency.

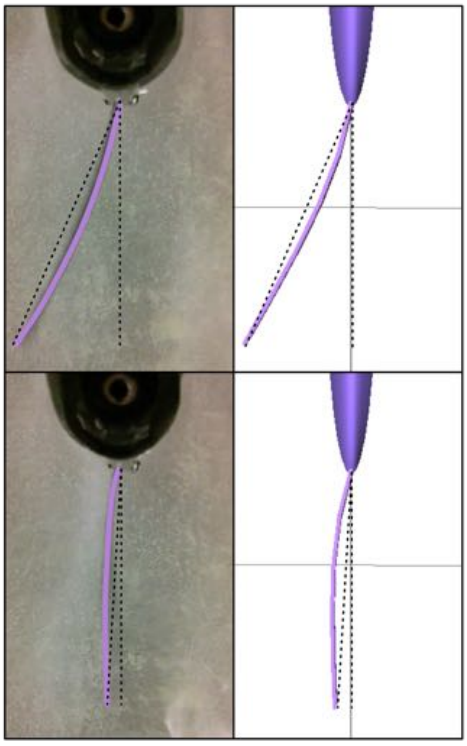

Fig. 11. Comparison between the motion of a caudal fin for physical (left) and virtual (right) experiments. To increase visibility, a purple line traces the length of the caudal fin for the physical device. The dashed, black reference lines provide a common angle with which the side-by-side images can be compared.

## VII. Conclusion

In this study, we applied evolutionary multiobjective optimization to the problem of balancing swimming performance and power efficiency in a robotic fish. Swimming performance is considered as maximizing the average speed, and power efficiency is calculated as the ratio between effective power and total power resulting from caudal fin actuation. While designing robotic fish is a well developed field of study, to our knowledge this is the first in which efficiency is co-optimized with swimming performance.

Results from NSGA-II evolutionary experiments provide insight into how a robotic fish should be designed for increased performance and efficiency. First, the control parameters (amplitude and frequency) should be set such that frequency is on the lower end of acceptable values and amplitude is on the

higher end of its range, while still providing enough thrust to reach the desired speed. Setting these parameters in such a way will lead to increased efficiency compared to using higher values for frequency with lower amplitudes. Second, the length-height ratio of the caudal fin should be approximately 3:1, and the length of the fin should be roughly half of the length of the body. Finally, caudal fins should be have a flexibility similar to rubber-like materials, as opposed to hard plastics. The conclusions drawn from these results are expected to generalize to any robotic fish of similar design, regardless of scale.

To verify that results from evolutionary simulation are physically meaningful, we fabricated several evolved fins and attached them to a robotic fish prototype. We utilized a multi-material 3D printer to fabricate fins made of composite materials, and based the evolutionary range of flexibilities on the capabilities of this printer. Experiments conducted in a water tank confirm that the evolved speeds correspond reasonably well with physical results. Further, through a visual comparison, we conclude that the total power of evolved solutions closely match reality, and thus, the solutions generated by NSGA-II constitute valid robotic fish designs. However, due to the clustering of evolved solutions, and the issues caused by the reality gap, trends among evolved solutions were lost when transfered to the physical device. In our ongoing research, we address this concern by combining evolutionary computation with adaptive control. While the multiobjective evolutionary design approach presented in this study was applied to a robotic fish, a similar approach can be applied to other physical systems.

## ACKNOWLEDGMENT

The authors gratefully acknowledge the contributions and feedback on the work provided by Jared Moore, as well as support from the BEACON Center at Michigan State University. This work was supported in part by National Science Foundation grants IIS-1319602, CCF-1331852, CNS-1059373, CNS-0915855, and DBI-0939454, and by a grant from Michigan State University.

## REFERENCES

[1] X. Tan, "Autonomous robotic fish as mobile sensor platforms: Challenges and potential solutions," *Marine Technology Society Journal*, vol. 45, no. 4, pp. 31–40, 2011.

[2] J. Yu, L. Liu, L. Wang, M. Tan, and D. Xu, "Turning control of a multilink biomimetic robotic fish," *IEEE Transactions on Robotics*, vol. 24, no. 1, pp. 201–206, 2008.

[3] A. J. Clark, J. M. Moore, J. Wang, X. Tan, and P. K. McKinley, "Evolutionary design and experimental validation of a flexible caudal fin for robotic fish," in *Proceedings of the Thirteenth International Conference on the Synthesis and Simulation of Living Systems*, East Lansing, Michigan, USA, July 2012, pp. 325–332.

[4] A. J. Clark and P. K. McKinley, "Evolutionary optimization of robotic fish control and morphology (poster summary)," in *Proceedings of the 2013 ACM Genetic and Evolutionary Computing Conference Companion*, Amsterdam, The Netherlands, 2013, pp. 21–22.

[5] J. D. Hiller and H. Lipson, "Automatic design and manufacture of soft robots," *IEEE Transactions on Robotics*, vol. 28, no. 2, pp. 457–466, 2012.

[6] C. Richter and H. Lipson, "Untethered hovering flapping flight of a 3D-printed mechanical insect," *Artificial Life*, vol. 17, no. 2, pp. 73–86, 2011.

[7] K. Deb, A. Pratap, S. Agarwal, and T. Meyarivan, "A fast and elitist multiobjective genetic algorithm: NSGA-II," *IEEE Transactions on Evolutionary Computation*, vol. 6, no. 2, pp. 182–197, 2002.

[8] E. Zitzler, M. Laumanns, and L. Thiele, "SPEA2: Improving the Strength Pareto Evolutionary Algorithm," Computer Engineering and Networks Laboratory (TIK), ETH Zurich, Zurich, Switzerland, Tech. Rep. 103, 2001.

[9] F. S. Hover, R. M. Eustice, A. Kim, B. Englot, H. Johannsson, M. Kaess, and J. J. Leonard, "Advanced perception, navigation and planning for autonomous in-water ship hull inspection," *International Journal of Robotics Research*, vol. 31, no. 12, pp. 1445–1464, 2012.

[10] Y. Wang, R. Tan, G. Xing, J. Wang, and X. Tan, "Accuracy-aware aquatic diffusion process profiling using robotic sensor networks," in *Proceedings of the 11th ACM/IEEE Conference on Information Processing in Sensor Networks*, Beijing, China, 2012, pp. 281–292.

[11] J. J. Faria, J. R. Dyer, R. O. Clément, I. D. Couzin, N. Holt, A. J. Ward, D. Waters, and J. Krause, "A novel method for investigating the collective behaviour of fish: introducing robofish," *Behavioral Ecology and Sociobiology*, vol. 64, no. 8, pp. 1211–1218, 2010.

[12] J. H. Long, Jr., T. J. Koob, K. Irving, K. Combie, V. Engel, H. Livingston, A. Lammert, and J. Schumacher, "Biomimetic evolutionary analysis: Testing the adaptive value of vertebrate tail stiffness in autonomous swimming robots," *Journal of Experimental Biology*, vol. 209, no. 23, pp. 4732–4746, 2006.

[13] M. S. Triantafyllou and G. S. Triantafyllou, "An efficient swimming machine," *Scientific American*, vol. 272, p. 64, 1995.

[14] J. M. Anderson and N. K. Chhabra, "Maneuvering and stability performance of a robotic tuna," *Integr. Comp. Biol.*, vol. 42, pp. 118–126, 2002.

[15] K. H. Low and C. W. Chong, "Parametric study of the swimming performance of a fish robot propelled by a flexible caudal fin," *Bioinspiration and Biomimetics*, vol. 5, no. 4, 2010.

[16] J. L. Tangorra, G. V. Lauder, I. W. Hunter, R. Mittal, P. G. A. Madden, and M. Bozkurttas, "The effect of fin ray flexural rigidity on the propulsive forces generated by a biorobotic fish pectoral fin," *Journal of Experimental Biology*, vol. 213, pp. 4043–4054, 2010.

[17] E. Kanso and P. K. Newton, "Passive locomotion via normal-mode coupling in a submerged spring-mass system," *Journal of Fluid Mechanics*, vol. 641, pp. 205–215, 2009.

[18] Y.-J. Park, U. Jeong, J. Lee, S.-R. Kwon, H.-Y. Kim, and K.-J. Cho, "Kinematic condition for maximizing the thrust of a robotic fish using a compliant caudal fin," *IEEE Transactions on Robotics*, vol. 28, pp. 1216–1227, 2012.

[19] P. V. Alvarado and K. Youcef-Toumi, "Design of machines with compliant bodies for biomimetic locomotion in liquid environments," *Journal of Dynamic Systems, Measurement, and Control*, vol. 128, pp. 3–13, 2006.

[20] K. H. Low and C. W. Chong, "Parametric study of the swimming performance of a fish robot propelled by a flexible caudal fin," *Bioinspiration & Biomimetics*, vol. 5, no. 4, 2010.

[21] C. J. Esposito, J. L. Tangorra, B. E. Flammang, and G. V. Lauder, "A robotic fish caudal fin: effects of stiffness and motor program on locomotor performance," *The Journal of experimental biology*, vol. 215, no. 1, pp. 56–67, 2012.

[22] N. Jakobi, P. Husbands, and I. Harvey, "Noise and the reality gap: The use of simulation in evolutionary robotics," in *Advances in Artificial Life, Lecture Notes in Computer Science*. Springer, 1995, vol. 929, pp. 704–720.

[23] J. Wang, P. K. McKinley, and X. Tan, "Dynamic modeling of robotic fish with a flexible caudal fin," in *Proceedings of the ASME 2012 5th Annual Dynamic Systems and Control Conference, joint with the JSME 2012 11th Motion and Vibration Conference, Ft. Lauderdale, Florida, USA*, 2012.

[24] M. Lighthill, "Large-amplitude elongated-body theory of fish locomotion," *Proceedings of the Royal Society of London. Series B. Biological Sciences*, vol. 179, no. 1055, pp. 125–138, 1971.

[25] S. Koos, J.-B. Mouret, and S. Doncieux, "Crossing the reality gap in evolutionary robotics by promoting transferable controllers," in *In Proceedings of the 12th Annual Conference on Genetic and Evolutionary Computation (GECCO)*. ACM, 2010, pp. 119–126.

[26] "Simulink: Dynamic system simulation for MATLAB, User's Guide," The MathWorks Inc., Natick, Massachusetts, USA, 1990-2013.